# Supporting Information

# Enhanced Stability and Lithium Storage Mechanism of Oxygen Vacancy-Induced Heterogeneous $Li_4Ti_5O_{12}/TiO_2$(B) Anolytes

Fengjie Zhang [a,b], Wenhao Fang [a,b], Xiangkun Wu [a,b], Xingmei Lu [a,b] *

[a] *Beijing Key Laboratory of Ionic Liquids Clean Process, CAS Key Laboratory of Green Process and Engineering, Institute of Process Engineering Chinese Academy of Sciences, Beijing 100190, PR China.*

[b] *School of Chemical Engineering, University of Chinese Academy of Science, Beijing, 100049, PR China.*

* Corresponding authors.

E-mail addresses: xmlu@ipe.ac.cn.

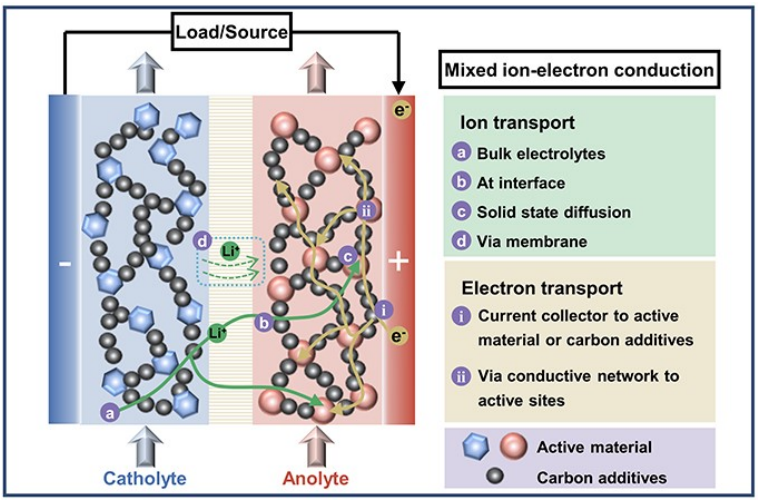


**Fig. S1 Diagram of a battery with anolyte and catholyte slurry assembly (including ion-electron transfer process inside)**

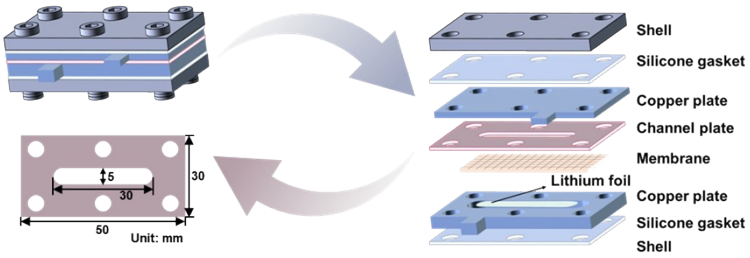


**Fig. S2 Schematic diagram of reactor design**

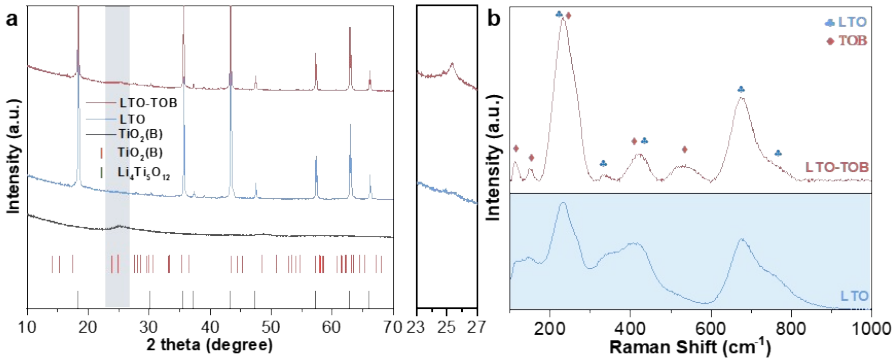


**Fig. S3 (a) XRD patterns and (b) Raman spectrums of LTO and LTO-TOB. (The heterostructure was characterized by GSAS II software, and the crystal structure parameters and peak shape parameters were constantly adjusted by the least square method, so that the calculated map and the experimental map reached a better coincidence degree. Upon importing the CIF files for LTO and $TiO_2$(B), the data underwent convergence through the refinement of parameters, including surface roughness, sample size, lattice dimensions, grain size, stress, and content. Consequently, the $R_w$ and GOF values in the comprehensive association variance outcomes fell below 10 and 1, respectively, signaling the completion of the fitting process)**

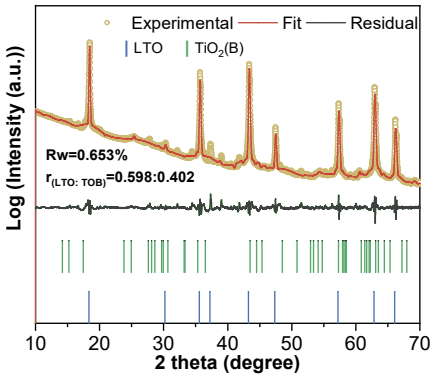


**Fig. S4 Result of the Rietveld refinement of the XRD pattern recorded for the LTO-TOB (the intensity is plotted in the log scale to increase the visibility of the $TiO_2$(B)-related reflections)**

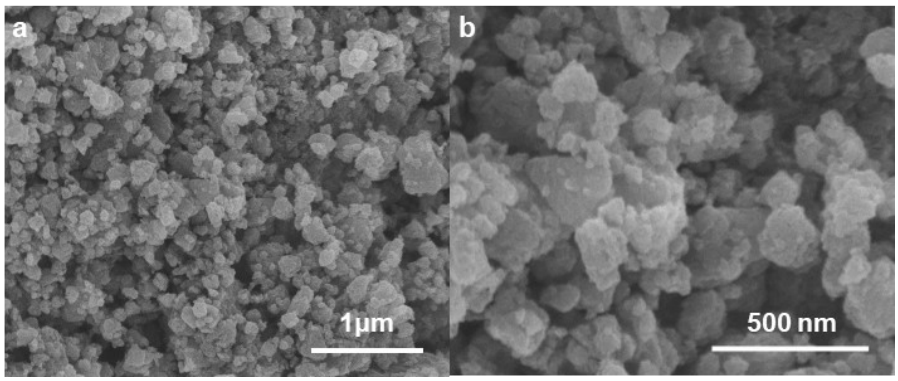


**Fig. S5 SEM images of (a, b) $TiO_2$(B)**

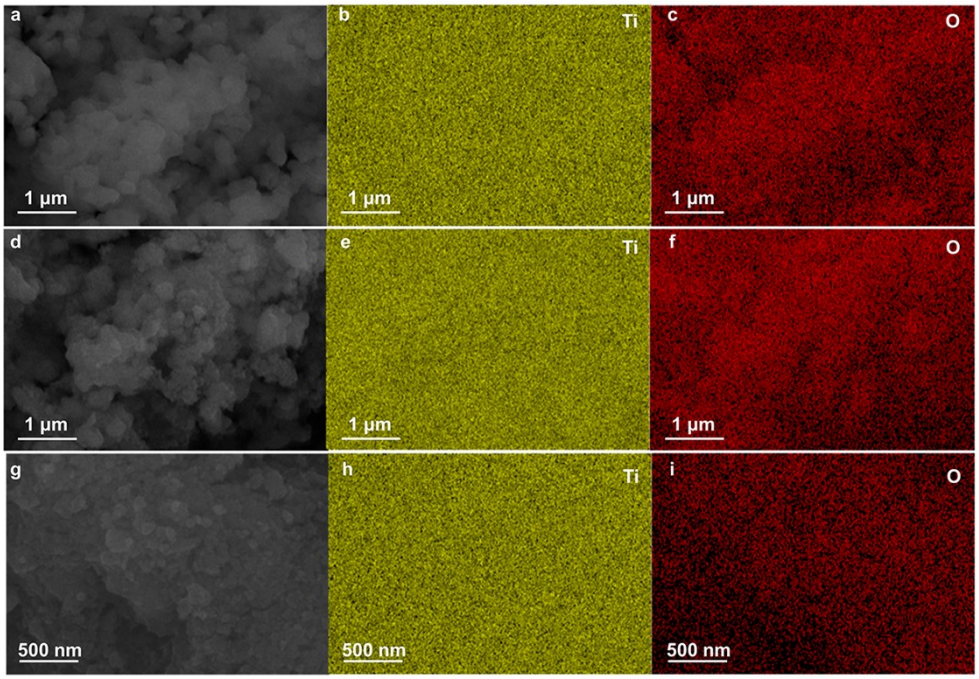


**Fig. S6 SEM images and elemental mapping images of (a-c) LTO, (d-f) LTO-TOB and (g-i) TOB**

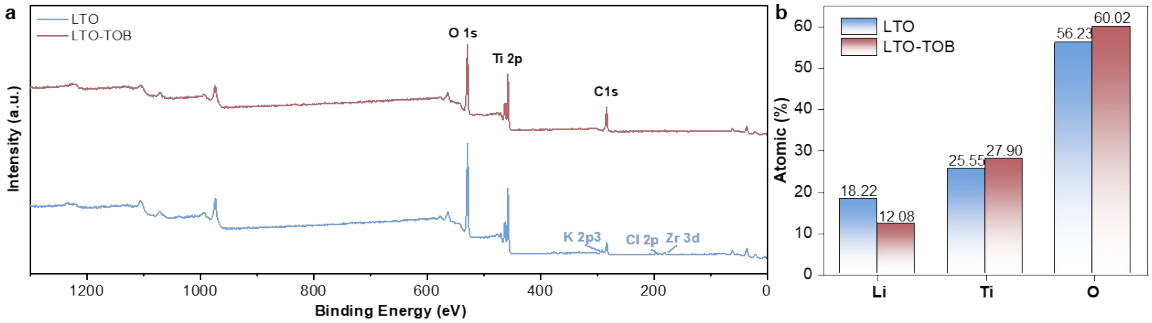


**Fig. S7 (a) XPS survey spectrum and (b) atomic percentage of LTO and LTO-TOB**

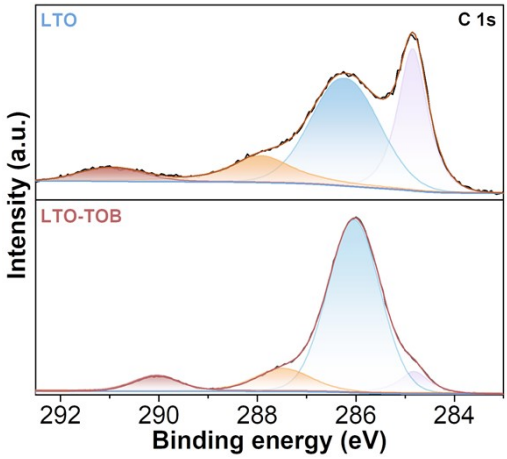


**Fig. S8 XPS spectra of LTO and LTO-TOB (C 1s) Before analyzing the Ti 2p and O 1s spectra, we calibrated the right-most (low-energy side) peaks to 284.8 eV according to the C 1s spectra, thus determining the charge shift of each element**

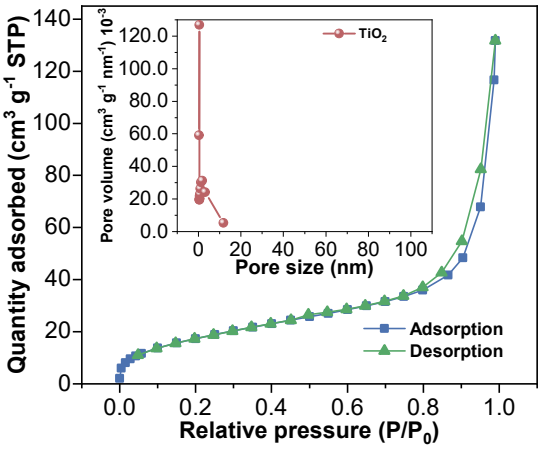


**Fig. S9 (a) The$N_2$ adsorption-desorption isotherms of $TiO_2$(B) (The specific surface area is 65.20 $m^2$ $g^{-1}$)**

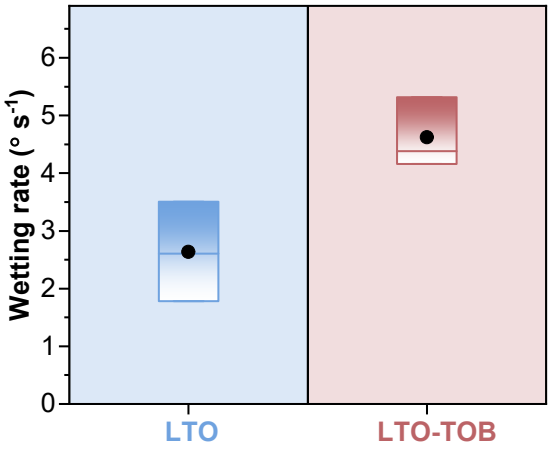


**Fig. S10 The wetting rate of the electrolyte on the surface of the active substance**

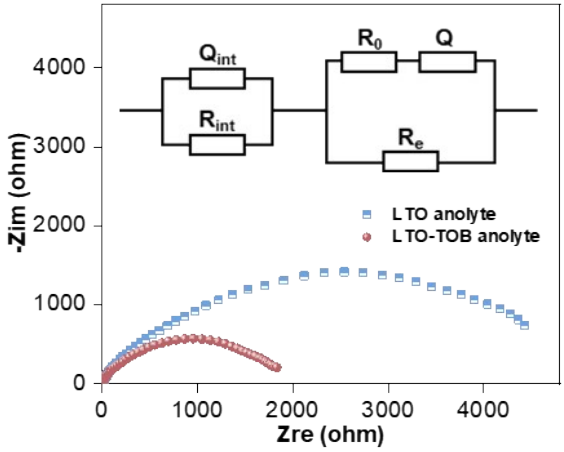


**Fig. S11 Nyquist plot, inset: Randles equivalent circuit of LTO and LTO-TOB anolyte ($R_{int}$, $R_0$, and $R_e$ represent interface impedance, slurry intrinsic resistance, and electron transfer resistance, respectively)**

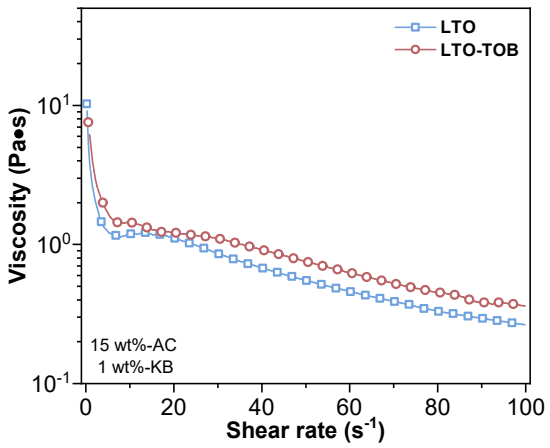


**Fig. S12 Shear viscosity of LTO and LTO-TOB slurry**

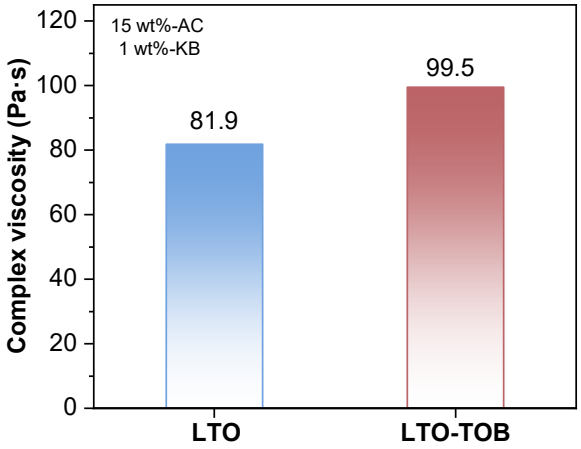


**Fig. S13 Complex viscosity of LTO and LTO-TOB slurry**

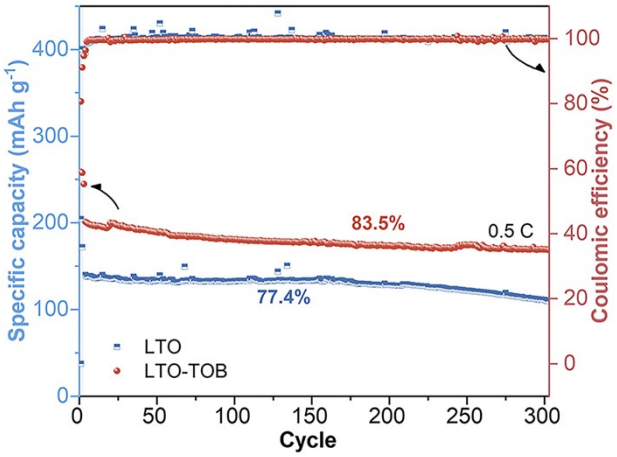


**Fig. S14 Long-term cycle performance of LTO and LTO-TOB slurry**

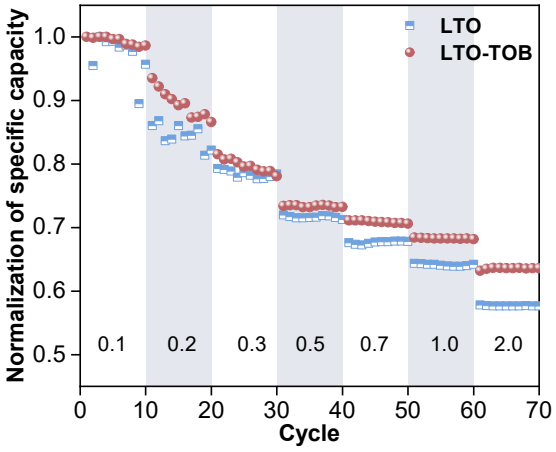


**Fig. S15 Normalization of rate performance of LTO and LTO-TOB anolyte**

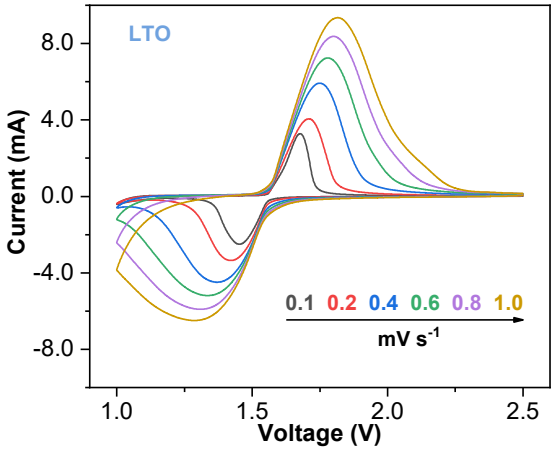


**Fig. S16 CV curves at different scan rates of LTO anolyte**

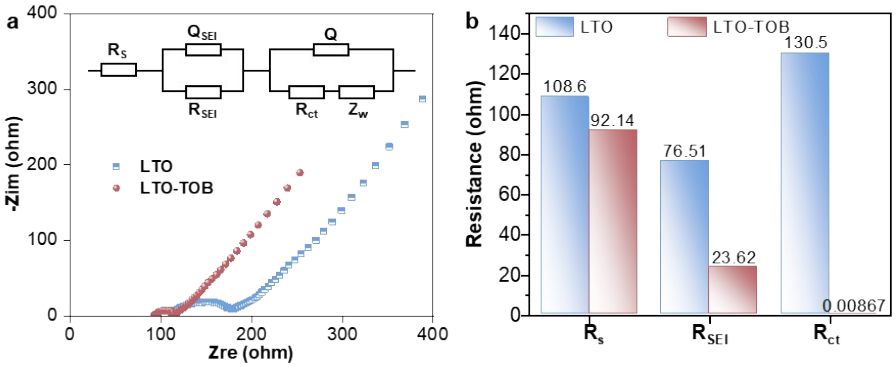


**Fig. S17 (a) Nyquist plots and the equivalent circuits of LTO and LTO-TOB anolyte (Rs, RSEI, and Rct stand for ohmic resistance associated with electrolyte resistance, solid electrolyte interface resistance, and charge transfer resistance, respectively). (b) The fitted results from Nyquist plots**

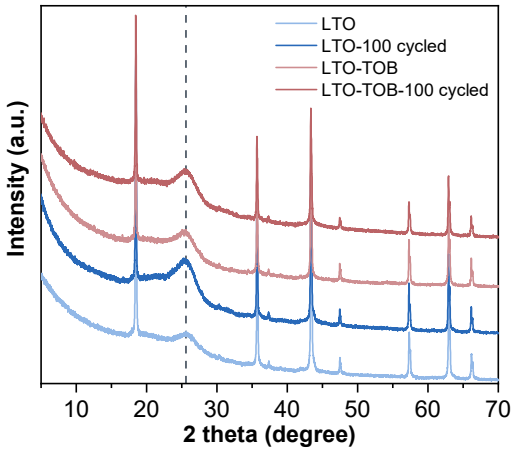


**Fig. S18 XRD diffraction spectrum of the slurry before and after 100 cycles**

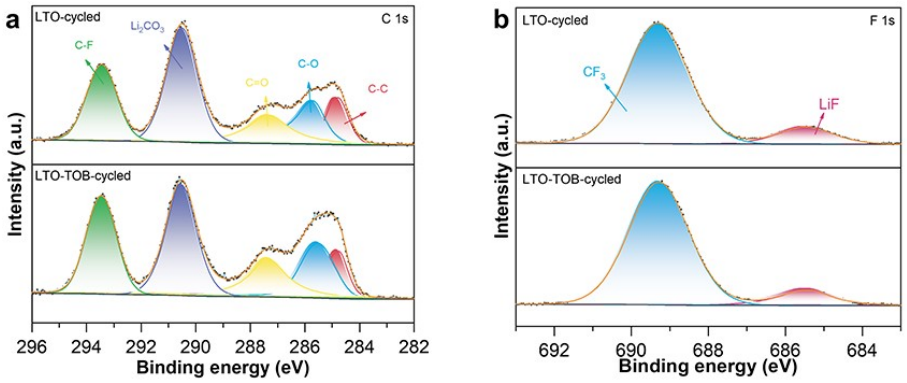


**Fig. S19 XPS spectra of LTO and LTO-TOB anolyte before and after 100 cycles for various elements including (a) Ti 2p and (b) F 1s**

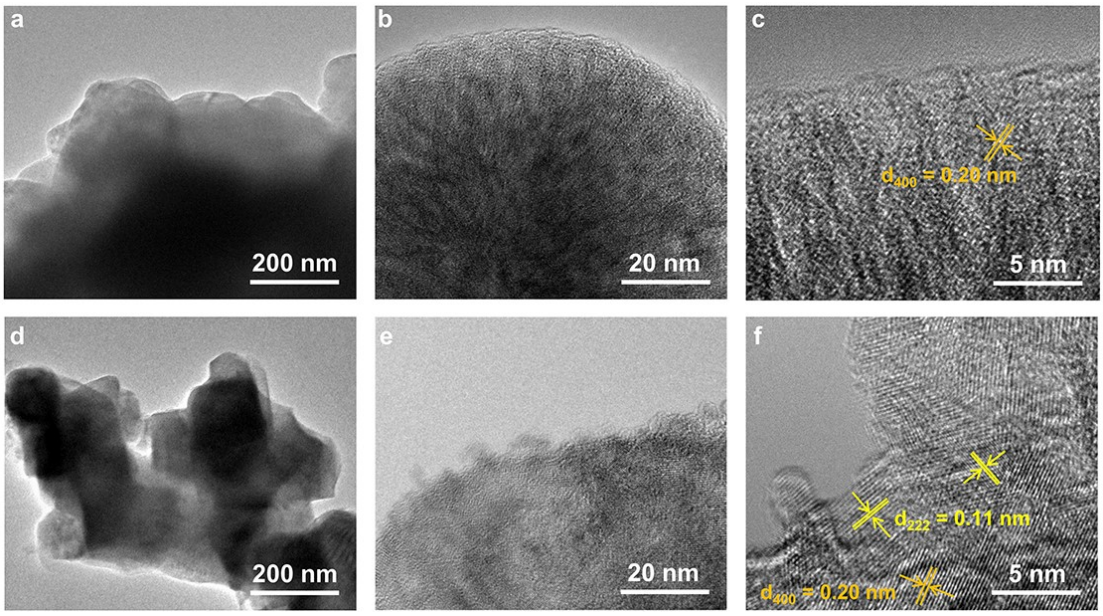


**Fig. S20 TEM images and corresponding elemental mappings of (a-c) LTO and (d-f) LTO-TOB slurry after 100 cycles at 0.5 C**

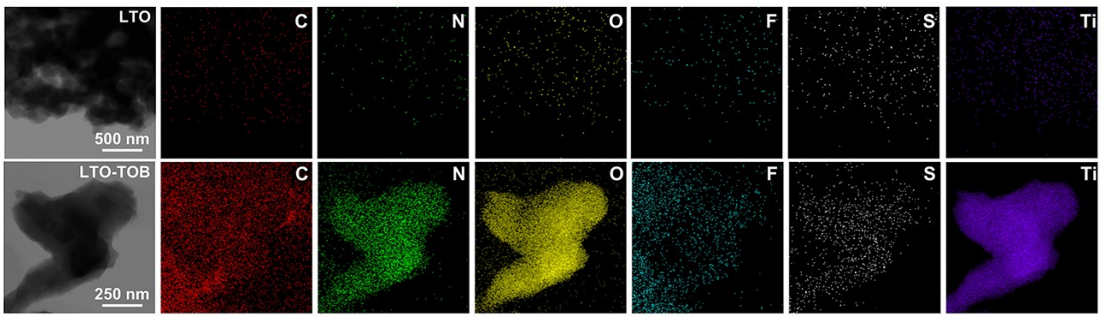


**Fig. S21 HAADF-STEM images and corresponding elemental mappings of LTO and LTO-TOB slurry after 100 cycles at 0.5 C**

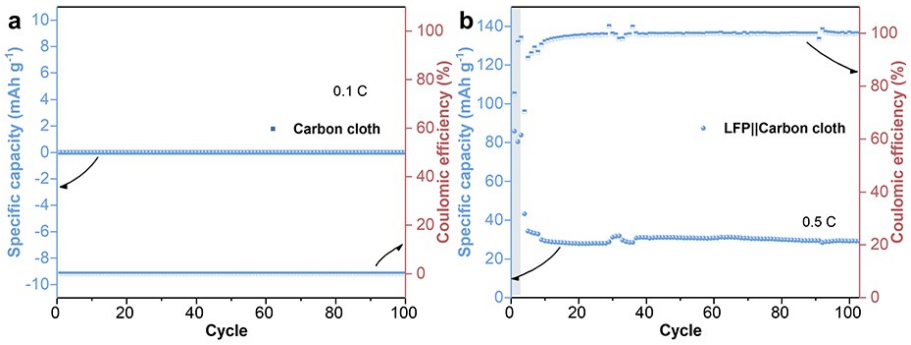


**Fig. S22 Electrochemical performance of carbon cloth assembled lithium half battery and LFP|| carbon cloth full battery with voltage range of 1.0~ 3.0 V**

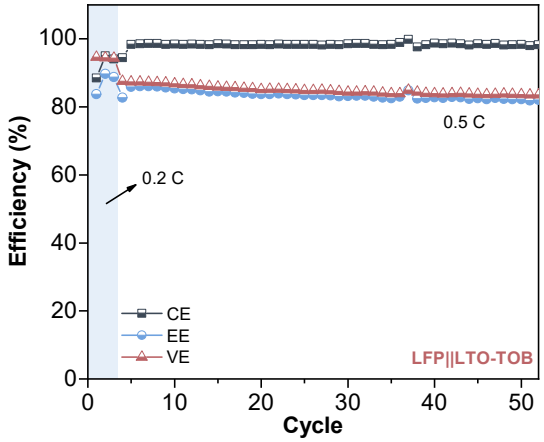


**Fig. S23 CE, VE and EE in the cycle of LFP||LTO-TOB full cell.**

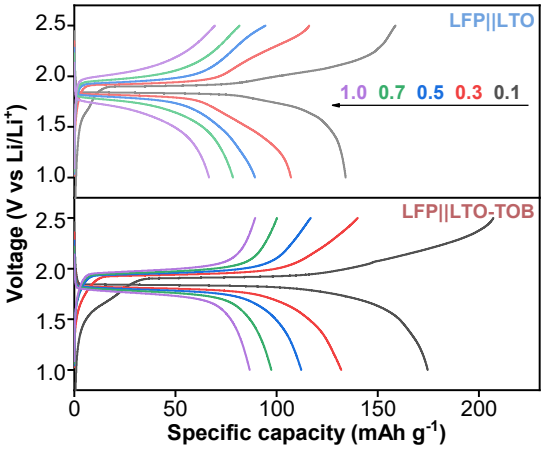


**Fig. S24 GCD curves at different current density of LFP||LTO and LFP||LTO-TOB full coin-cell.**

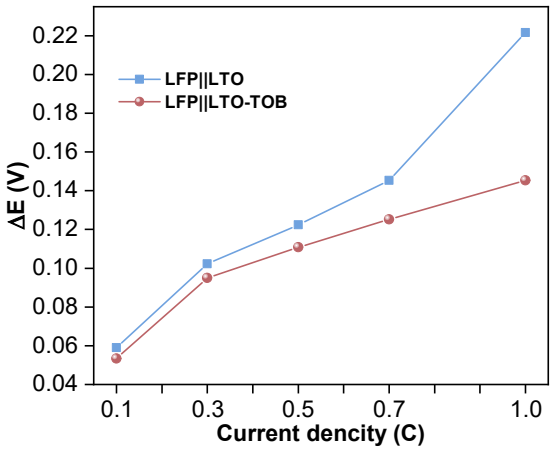


**Fig. S25 Voltage platform difference of charge and discharge (ΔE) at different current density of LFP||LTO and LFP||LTO-TOB full coin-cell**

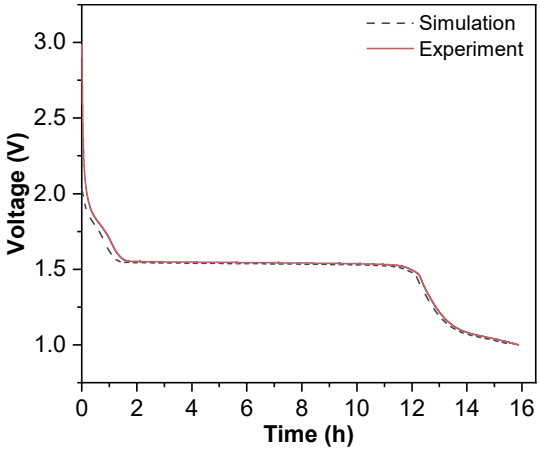


**Fig. S26 Voltage curve of the discharge process of the slurry reactor (the lithiation process): experimental and simulated data**

## Section I Calculation of electronic conductivity

**Calculation formula：**

$$\sigma = \frac{L}{S \times R_e}$$

σ, L, S, and $R_e$ in the above formulas represent the electron conductivity, thickness of slurry, effective contact area, and electron transfer resistance, respectively.

## Section II Electrochemical reaction kinetics -*b* value

### Power law relation

$i = av^b$ The *i* and *v* in the formula represent the peak current and the sweep speed respectively. When *b* is 0.5, it represents the diffusion control behavior in the battery, and when *b* is 1, it represents the surface-controlled pseudo-capacitance behavior in the battery.

## Section III Calculation of $Li^+$ diffusion coefficient

### i. Cyclic voltammetry (CV):

**Calculation equation: Randle-Sevcik equation**

$$i_p = \left(2.69 \times 10^5\right) n^{3/2} A D_{Li^+}^{1/2} C_{Li^+} v^{1/2}$$

$i_p$ stands for peak current, while $D_{Li+}$ and $C_{Li+}$ stand for $Li^+$ diffusion coefficient and volume concentration respectively. $n$ is the stoichiometric number of electrons in the electrode reaction; $A$ represents the area of the electrode. The slope of the linear relationship that can be fitted according to $i_p$ and $v^{1/2}$ is positively related to the lithium-ion diffusion coefficient.

### ii. Electrochemical Impedance Spectroscopy (EIS):

**Calculation equation:**

$$Z_{Re} = R_{CT} + R_S + R_{SEI} + \sigma\omega^{-1/2} \qquad D_{Li^+} = \frac{R^2T^2}{2A^2n^2F^4C_{Li}^2\sigma^2}$$

The real part impedance $Z_{re}$ and angular frequency $\omega^{-1/2}$ of the Nyquist plot at low frequency are linearly fitted according to the above Equation 4 to get the slope σ, which is the Warburg factor. In Equation 5, $R$ is the gas constant, $T$ is the absolute temperature, $A$ represents the electrode surface area, $n$ is the number of electrons transferred, $F$ is the Faraday constant, $D_{Li+}$ and $C_{Li+}$ represent the $Li^+$ diffusion coefficient and concentration. The square of the Warburg factor is negatively correlated with the $D_{Li+}$.

### iii. Galvanostatic Intermittent Titration Technique (GITT):

**Calculation equation: Fick's second law**

$$D_{Li^+} = \frac{4}{\pi}\left(\frac{m_B V_M}{M_B A}\right)^2\left(\frac{\Delta E_S}{\tau\left(dE_\tau/d\sqrt{\tau}\right)}\right)^2\left(\tau \ll \frac{L^2}{D_{Li^+}}\right)$$

In the above formula, $V_M$, $M_B$, and $m_B$ represent the molar volume, molecular weight, and mass of the active material, respectively; $L$ and $A$ are the electrode thickness (lithium diffusion distance) and electrode area, respectively; $\tau$ is the duration. If the battery voltage change with duration is linear on the $\tau^{1/2}$ curve, then **equation 6** may be simplified as follows:

$$D_{Li^+} = \frac{4}{\pi\tau}\left(\frac{m_B V_M}{M_B A}\right)^2\left(\frac{\Delta E_S}{\Delta E_\tau}\right)^2\left(\tau \ll \frac{L^2}{D_{Li^+}}\right)$$

## Section IV Modeling of slurry battery

Newman et al. failed to consider the real geometric properties of porous electrode in the porous electrode theory. Every part of the electrode contains a solid-liquid two-phase, which can be expressed as a continuous function in time and space. All features are the superposition of continuous function sets within two-phase. Despite the active component of the slurry battery, unlike lithium-ion batteries, is not fixed but continuously mixed with the electrolyte and flows, the overall static flow channel still adheres to the Newman porous electrode theory, allowing for its application in solving the associated problems. The current conservation and mass balance of the slurry

electrode reaction can be described as follows:

$i_s = -\sigma_{s,eff}\nabla\phi_s i_1 = -\sigma_{l,eff}\nabla\phi_l + (2\sigma_{l,eff}RT/F)(1 + \partial lnf/\partial lnc_l)(1 - t_+)\nabla lnc_l$

$\partial\varepsilon_l c_l/\partial t + \nabla\cdot(-D_{l,eff}\nabla c_l + i_l t_+/F) + u_l \cdot \nabla c_l = R$ $\sigma_{s,eff}$, $\phi_s$ and $\varepsilon_s$ are effective conductivity, potential and volume fraction of solid-phase. $\sigma_{l,eff}$, $\phi_l$, and $\varepsilon_l$ are effective conductivity, potential and volume fraction of liquid - phase. $f$ and $D_{l,eff}$ are activity coefficient and effective diffusion coefficient of electrolyte. $R$, $t$, $t^+$ and $F$, are universal gas constant, temperature, migration number of $Li^+$ and Faraday constant.

The equilibrium potential of lithium intercalation reaction can be determined by SOC, and the lithium diffusion process inside the particles is described by Fick 's second law:

$\partial c/\partial t = D_s(\partial^2 c/\partial r^2 + 2\partial c/(r\partial r))$ The local current density caused by the intercalation reaction is determined by the electrode surface reaction rate, according to the Butler-Volmer equation:

$i_{loc} = i_0(exp(\alpha_a F\eta/(RT)) - exp(-\alpha_c F\eta/(RT)))$ $i_0$ is the exchange current density, $\alpha_a$ and $\alpha_c$ are the anode and cathode transfer coefficients, and the overpotential $\eta$ is:

$\eta = \phi_s - \phi_1 - E_0$ Like lithium-ion batteries, there is no electrochemical reaction in the separator, $c_l$ and $\phi_l$ are the only relevant variables:

$$\nabla\left(k_{eff}\nabla\phi_l - kRT/F(1 - t_+^0)\nabla lnc_l\right) = 0 \partial c_l/\partial t = \nabla(D_{eff}\nabla c_l)$$

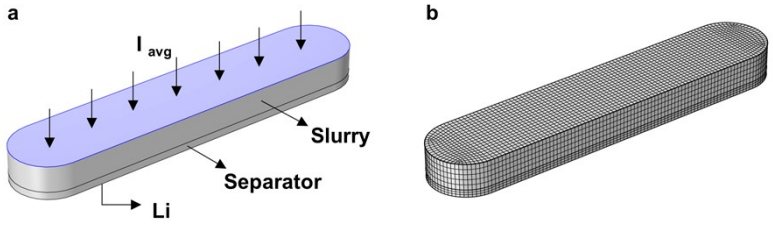


**Fig. S19 (a) Computational domain of slurry half-cell; (b) Grid of slurry half-cell.**

**Table S1 Kinetic, electrochemistry and operating parameters used in the simulation.**

| Symbol | Parameter | Value |
|---|---|---|
| $r_{LTO}$ | Radius of LTO particles | 2.37 μm |
| $\rho_{LTO}$ | Density of LTO particles | 3400 kg $m^{-3}$ |
| $\phi_l$ | Initial volume fraction of liquid phase | 0.86571 |

| | | |
|---|---|---|
| $\phi_d$ | Initial volume fraction of solid phase | 0.13429 |
| $\sigma_l$ | Conductivity of liquid phase | 0.95 S $m^{-1}$ |
| $\sigma_s$ | Conductivity of solid phase | 100 S $m^{-1}$ |
| $D_l$ | Diffusion coefficient of liquid phase | $4.038\times10^{-10}$ $m^2$ $s^{-1}$ |
| $D_s$ | Diffusion coefficient of solid phase | $6.8\times10^{-15}$ $m^2$ $s^{-1}$ |
| $c_{s,max}$ | Reference Lithium concentration | 22852 mol $m^{-3}$ |
| $t_+$ | Transport number for $Li^+$ | 1 |
| $\alpha_a$ | Transfer coefficient of anode | 0.5 |
| $\alpha_c$ | Transfer coefficient of cathode | 0.5 |
| $h_m$ | Thickness of the membrane | 0.1 mm |
| $\varepsilon_m$ | Porosity of the membrane | 0.55 |
| $i_0$ | The exchange current density | 1 A $m^2$ |
| $T$ | System temperature | 298 K |
| $i_c$ | Applied current density | 0.5 mA $cm^2$ |
| $c_{s0}$ | Initial concentration of LTO | 228.52 mol $m^3$ |
| $c_{l0}$ | Initial electrolyte salt concentration | 1000 mol $m^3$ |